Sonochemical synthesis of aluminium and aluminium hybrids for remediation of toxic metals

Kousar Parveen[a,*], Uzaira Rafique[a], Muhammad Javed Akhtar[b], Muthupandian Ashokkumar[c]

[a] Department of Environmental Sciences, Fatima Jinnah Women University, The Mall, Rawalpindi 46000, Pakistan
[b] Physics Division, PINSTECH, P.O. Nilore, Islamabad, Pakistan
[c] School of Chemistry, University of Melbourne, Australia

ABSTRACT

Spherical shaped nano-size aluminium oxide and its hybrids with indole and indole derivatives have been synthesized using sol–gel and post grafting methods coupled with sonication (Branson Digital SonifierS-250D; 20 kHz; 40%) for the remediation of toxic metals (lead and mercury). Different spectroscopic techniques (FTIR, SEM, BET, XRD, and XPS) have been applied to assess the properties of synthesized aluminium oxide and its hybrids. FTIR spectra showed the absorption bands of aluminium oxide (Al-O-Al) and aluminium hybrids (Al-O-C) at 800–400 cm^{-1} and 1650–1100 cm^{-1} region, respectively. SEM showed spherical shaped clusters of aluminium oxide which changed into the net-shape structure after the hybrid synthesis. It is worth noting that sonication energy increases the total surface area of aluminium oxide when it gets hybridized with indole and its derivatives from 82 m^2/g to 167 m^2/g; it also improved the product yield from 68% to 78%. Simultaneously, FTIR, SEM and BET analysis of non-sonicated aluminium oxide and its hybrids were also recorded for comparison. While XRD and XPS analysis were only conducted for sonicated aluminium oxide and its hybrids to manifest the structural and compositional properties. XRD patterns indexed as the cubic crystal system with an average 41 nm crystallite size of sonicated aluminium oxide which remains unaffected after hybrid synthesis. A survey scan under XPS confirmed the presence of all expected elements (aluminium, oxygen, carbon, nitrogen) and deconvolution of each recorded peak showed binding of element with its neighboring elements. The performance of aluminium oxide and its hybrids synthesize with and without sonication are also evaluated using a time-dependent batch adsorption protocol optimize for one hour. The maximum adsorption of lead (37%) and mercury (40%) are found onto sonicated aluminium oxide. The sonicated aluminium hybrids showed 43–63% of lead and 55–67% of mercury at pH 7. The fitness of experimental data using adsorption kinetics and isotherms revealed that adsorption follows Pseudo-second-order kinetic, Langmuir, and Freundlich isotherms.

1. Introduction

The excessive release of untreated industrial effluents in water bodies drastically impact the quality of drinking water. People rely on consuming contaminated water and suffer from water-borne diseases worldwide. According to the statistic of the World Wide Fund (2005) and Pakistan Council of Research in Water Resources (2010), only 25.61% (including 23.5% rural and 30% urban) of Pakistani population have access to safe and drinkable water [1]. Furthermore, water borne diseases are responsible for one-third of all deaths and cause an income loss of 25–58 billion rupees, i.e., 0.6–1.44% of Pakistan's GDP. To address these alarming issues, different organizations like Pakistan Council of Research in Water Resources (PCRWR), Pakistan Standards and Quality Control Authority (PSQCA), Ministry of Climate Change, Ministry of Health and Environmental Protection Agency are working effectively and devised set the standards for safe

drinking water [2]. Existing wastewater treatment methods include chemical precipitation, coagulation, ion-exchange and electrochemical deposition, have high operational cost, high energy consumption and produce toxic sludge, which requires further treatment. Adsorption emerged as an alternate method as it is easier to operate, consumes less energy, low operational cost, and a variety of adsorbent which can be regenerated and reused in multiple of times [3]. Considering these advantages, scientists widely studied the adsorption method as a tool for the remediation of noxious metals from industrial effluents. Aluminium oxide emerged as fascinating versatile material [4] with its intrinsic properties such as polymorphism, chemical and mechanical stability, low thermal conductivity, porosity, high surface to volume ratio and amphoteric nature [5]. These diverse properties of aluminium oxide provided enough room to be applied in various applications, such as adsorbent, catalyst, filler and electric insulator, etc. Aluminium oxide can be synthesized by diverse methods like

---

* Corresponding author.
  E-mail address: kosar_ahmed111@yahoo.com (K. Parveen).

precipitation [6], sol–gel [7], hydrothermal [8], solvothermal [4] and direct thermal treatment [9]. However, limitations of these methods such as long reaction time, uncontrolled particle size, high-temperature requirement, use of expensive and toxic organic solvents and salts [10] placed great demand for the new synthetic method which is economical and efficient. The sonochemical method emerged as a facile, efficient and environmental benign route due to less energy consumption, short reaction time and an alternate option for tuning the desired shape and size-controlled properties [11]. The main working principle behind the sonication is the generation of active radicals through the formation, growth and implosion of acoustic cavitation. Suslick [12] reported that the collapse of acoustic cavitation produces intense local high temperature (~5000 K), high pressures (~1000 atm.) with enormous heating and cooling rates ($> 10^9$ K/sec) and liquid jet streams (~400 km/h). Thus this condition favors initiating the chemical reaction within the respective media. Previously it has been observed that sonication works efficiently for the synthesis of metal oxides and metal hybrid. Luévano-Hipólito and Torres-Martínez [13] synthesized the zinc oxide using a sol–gel method assisted with sonication (26 kHz; 150 W) from 0 to 60 min to test the photocatalytic hydrogen production. The result showed 10^7 μmol $g^{-1}h^{-1}$ of hydrogen production. Hassanjani-Roshan et al., [14] synthesized iron oxide from $FeCl_3 \cdot 6H_2O$ and NaOH. The high-energy sonication waves (20 kHz) were applied for 1 h which yield spherical particles with crystallite size between ~5 and ~7.5 nm. Cui et al., [15] synthesized the graphene oxide wrapped gold nanoparticles using the sonochemical method for the photocatalysis of rhodamine B. The graphene oxide wrapped gold nanoparticles were sonicated (200 W) for 1 h. It showed good photocatalytic activity under visible light and decompose rhodamine B in 2 h. Lee et al., [16] synthesized the copper-doped bismuth vanadate/graphitic carbon nitride nanocomposite using a sonochemical method. The reaction mixture was sonicated (700 W, 20 kHz) for 0.5 − 1 h, and used the synthesized nanocomposite as a photocatalyst for the degradation of the Bisphenol A. The results showed that the nanocomposite improved the electron/hole pair separation, stability and light-harvesting efficiency in comparison to the pristine bismuth vanadate or graphitic carbon. It completely degrades the Bisphenol A after 90 min. Similarly, Dezfuli et al., [17] synthesized ceria reduced graphene oxide nanocomposite after sonication (400 W, 24 kHz) for 88 min. These results showed that the cerium oxide nanoparticles were anchored on graphene oxide, the synthesized nanoparticles were applied as an electro-catalyst. Table 1 shows the previously reported literature on the aluminium oxide and its composites with different sonication treatments.

Hence, the literature review showed that sonication treatment is proved to be a very effective method for the synthesis of different metal oxides and metal composites. Therefore, the present research is designed to synthesize aluminium oxide and aluminium hybrids using sol–gel and post-grafting assisted with sonochemical method. To best of our knowledge, the present study is the first attempt to synthesize aluminium hybrids using indole and its derivatives and applied as an adsorbent for metal remediation. The indole group is an important class of heterocyclic compounds due to its unique structure. It has π-electron and lone pair at C_2, C_3, and N_1 positions of indole which provides reactive sites to electrophiles and nucleophilic substitution. It is less toxic, thermally stable, and present in the structure of

many natural products such as amino acid, auxin. It also exhibits metal-binding properties. For this purpose, aluminium nitrate nano-hydrate and ammonia solution were used as the starting materials for the synthesis of aluminium oxide by employing a sonochemical assisted sol–gel method. Then 1:2 (w/w) ratio of aluminium oxide and indole group were hybridized using post grafting method with aid of sonication. The effects of sonication treatment on the internal and outer structural properties of aluminium were recorded and compared with non-sonicated aluminium hybrids.
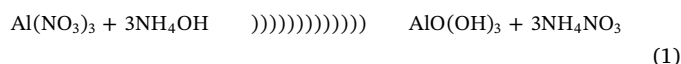
2. Experimental Details

2.1. Reagents:

Aluminium nitrate nano-hydrate (99.9%), 3-aminopropyltiethoxysilane (99%), indole (≥99%), indole-2 carboxylic acid (98%), 2-methyl indole (98%), lead nitrate (≥99.9%) and mercury nitrate monohydrate (≥99.9%) were purchased from Sigma-Aldrich Co. LLC (Australia). Ammonium solution (28%), acetonitrile (> 99.9%) and dichloromethane (≥99.9%) were purchased from Merck. All the chemical reagents were of analytical grade and used without any further purification.

2.2. Methods

2.2.1. Synthesis of aluminium oxide

Aluminium oxide was synthesized using a sol–gel assisted sonochemical method [19]. For this purpose, 0.1 M aluminium nitrate nano-hydrate solution was prepared in Milli-Q water and a 10% ammonium solution was added dropwise until the pH was adjusted to 8. Then the solution was ultra-sonicated using a Branson Digital SonifierS-250D (13 mm tip diameter, 20 kHz, 40%) for 1 h at room temperature. The horn tip is immersed 1 cm into the solution. After sonication, the solution was aged, centrifuged (6500 rpm for 20 min) to separate the solid product, washed, dried and calcined at 500 °C with a ramp rate of 10 °C/minute for 4 h. The 40% amplitude power dissipation in Milli-Q water is optimized using the Weissler method (see supplementary file). The product obtained was coded as S-Al. Similarly, the aluminium oxide was also synthesized using a sol–gel method without sonication. The solution was left undisturbed (24 h) for Ostwald ripening, centrifuged (6500 rpm for 20 min) to separate the solid product, dried and calcined at 500 °C with a ramp rate of 10 °C/minute for 4 h. The product obtained was coded as NS-Al. The reaction 1 and 2 illustrates the chemical reactions involved in the formation of aluminium oxide.

$$Al(NO_3)_3 + 3NH_4OH \quad))))))))))))) \quad AlO(OH)_3 + 3NH_4NO_3 \tag{1}$$

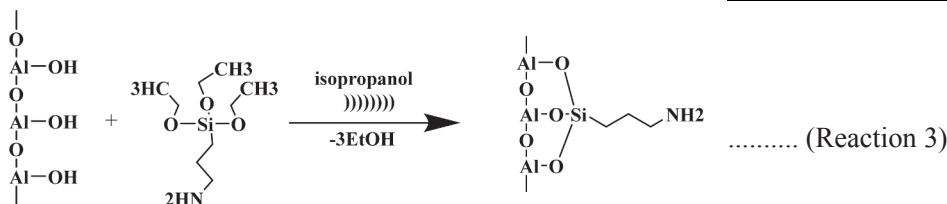$$2AlO(OH)_3 \xrightarrow[500°C]{} Al_2O_3 + 3H_2O \tag{2}$$

2.2.2. Synthesis of aluminium hybrids

Aluminium hybrids were synthesized using a post grafting method as reported earlier [26,27]. Briefly, as synthesized S-Al_2O_3 was charged
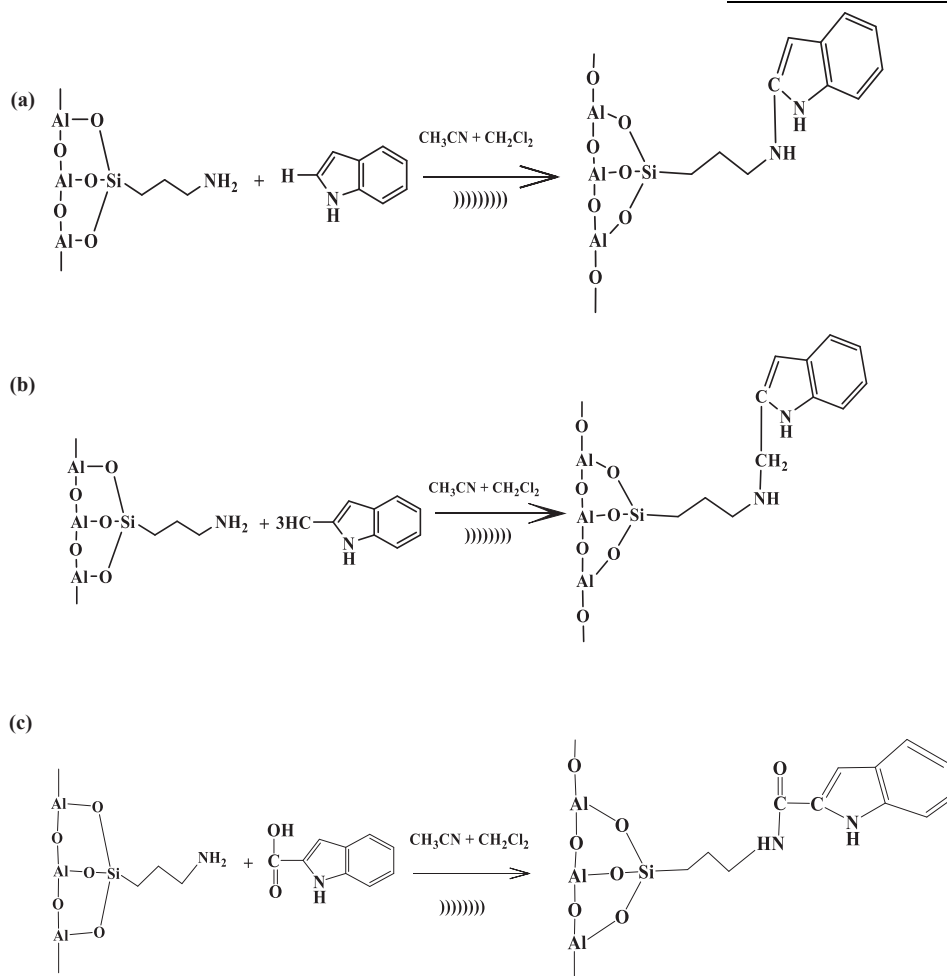
Table 1
Aluminium and its different composites reported previously.

Metal composites	Sonication treatment	Application	References
Aluminium sphere loaded with palladium	20 kHz; 100 W	Catalyst	Gaudino et al., [18]
Mesoporous aluminium oxide	20 k Hz; 30 W		Chave et al., [19]
Copper aluminate	20 k Hz ; 100 W	Catalyst	Lv et al., [20]
Nano-magnesia/ alumina	24 kHz ; 600 W	Adsorbent	Nazari and Halladj, [21]
Mesoporous γ alumina	20 kHz; 125 W	Catalyst	Segal et al., [22]
Polystyrene/ alumina	58 kHz ; 192/58 kHz; 430 kHz; 470 kHz; 1 MHz	Filler	Philip et al., [23]
Zirconium oxide-alumina / Graphene oxide	20 k Hz; 100 W	Adsorbent	Wang et al., [24]
Nickel Molybdenum /γ-alumina	20 k Hz; 90 W	Catalyst	Ameen et al.,[25]
The present work: Aluminium hybrids with indole; 2-methyl indole and carboxylic acid-2- indole	20 k Hz; 40 W	Adsorbent for Lead and mercury	————

with a 10% solution of 3-aminotriethoxypropylsilane (APTES) in isopropanol as shown in the reaction 3. The solution was sonicated, as described for aluminium oxide. Then filtered, and washed repeatedly with isopropanol and ethanol, centrifuged, dried and stored until further use. APTES was used as a bridging agent for effective chemical integration between aluminium oxide with indole and its derivatives.

Reaction 4: Aluminium-indole (a), aluminium-methyl indole (b) and aluminium-carboxylic indole (c) hybrids

2.2.3. Instrumentation

Different analytical instruments (FTIR, SEM, BET, XRD and XPS) were employed to characterize the synthesized products. Standard KBr

.... (Reaction 3)

An amount (0.15 g) of amine-functionalized aluminium oxide was dispersed in 20 ml of dichloromethane in a reagent flask for 15 min, filtered and dried. Then the indole solution (0.30 g in 20 ml acetonitrile) was added to it and sonicated for 1 h (as described earlier). The 40% amplitude power in dichloromethane is selected as the best power dissipated to the solution and where a high concentration of radicals is generated (see supplementary file). The synthesized aluminium hybrid was filtered and dried in air. Same procedure was also repeated for two other indole derivatives (indole-2 carboxylic acid, 2-methyl indole) as shown in reaction 4. A total of three hybrid products were obtained and coded as S-AI, S-AlCI, and S-AlMI. In the same way, aluminium hybrids were also synthesized using post grafting method without sonication and coded as NS-AlIN, NS-AlCI, and NS-AlMI.

pellet method was used to record FTIR spectra (averaged 15 scans) with a resolution sweep rate of 4 cm^{-1} from 4000 to 400 cm^{-1} using a clean cell window for background and air as reference. Scanning Electron Microscopy (Quanta 200 FEI) operated under 10 kV voltage and distance of 10 mm. Gold sputtering was used to prevent sample charging and placed on a thin film of carbon tape mounted on the stub. Air pulse was applied to remove excess and loose samples and then placed inside a vacuum chamber under argon. XRD data were collected from 5° to 80° with a step size of 0.02° (using Bruker D8 X-Ray diffractometer) having Cu-Kα radiation (1.54056 Å). Brunauer–Emmett–Teller (Micrometrix Tristar 3000) with multi-point nitrogen adsorption–desorption method

Table 2
Linearized equation of Adsorption kinetics and isotherms.

Linearized Equation	Parameters	Plot
Adsorption Kinetics		
Pseudo-first-order $\log (q_e - q_t) = \log (q_e) - (k_1 /2.303)t$	k_1 (slope) is rate constant (min^{-1}); qe (intercept) is adsorption capacity (mg g^{-1}) at equilibrium.	$\log(q_e - q_t)$ versus t
Pseudo-second-order $(t/q_t) = (1/k_2 q_e^2) + (1/q_e)t$	k_2 (slope) is rate constant (min^{-1}); q_t (intercept) is adsorption capacity at time t (mg g^{-1}).	t/q_t versus t
intra-particle diffusion $q_t = K_{id} t^{1/2} + C$	Kid (slope) is intraparticle diffusion rate constant (mg g^{-1} min$^{1/2}$);C (intercept) is the boundary layer thickness.	q_t versus t
Adsorption isotherm		
Langmuir $1/qe = 1/qmKL + 1/qmK_LCe$	Ce is metal concentration at equilibrium (mg L^{-1}); qe is metal adsorbed per unit mass (mg/g), qm (1/slope) is max. adsorption capacity (mg g^{-1}), K_L (intercept) is langmuir constant.	$1/q_e$ versus $1/C_e$
Freundlich $\log qe = \log K_F + (1/n) \log Ce$	K_F (intercept) is freundlich capacity; n (slope) is freundlich intensity.	log q_e versus log C_e

under 77 K and relative pressure (0.01–0.995) was used. Each sample was degassed at 423 K for 24 h on the vacuum line and pore size distribution was calculated from the Barret-Joyner-Halenda isotherm. X-ray photoelectron spectroscopy (Kratos Axis ULTRA; Thermo Scientific) equipped with analyzer (165 mm hemispherical electron energy) and monochromatic Al X-rays (1486 eV at 150 W) was used. The chamber and sample were placed under 1×10^{-9} torr and 1×10^{-8} torr, respectively. The survey scan was taken at 160 eV over 1200–0 eV with 1000 meV steps and dwell time of 100 ms. The curve fitting and deconvolution were performed using CasaXPS 2.3.15 software.

2.2.4. Batch adsorption experiments

Time-dependent batch experiments were designed for 60 min to test adsorption of selected toxic metals (Pb and Hg) as a function of pH (5 as acidic, 7 as neutral and 9 as basic), and concentration (30 mg/L, 40 mg/L and 50 mg/L for Pb while 30 µg/L, 40 µg/L and 50 µg/L for mercury). For each batch, a known concentration of synthetic adsorbate solution was pipetted out into eight separate vials containing a known amount (30 mg) of the adsorbent. After contact of five minutes between adsorbent and adsorbate, the solution was centrifuged and the supernatant was analyzed in flame atomic absorption (Varian Spectra *AA* 220) spectrophotometer. The adsorbed concentration per unit mass of the adsorbent (qe) was calculated using Eq. (1). Furthermore, the adsorption efficiency (% A) of sonicated aluminium oxide and its hybrids as adsorbent was calculated by using Eq. (2).

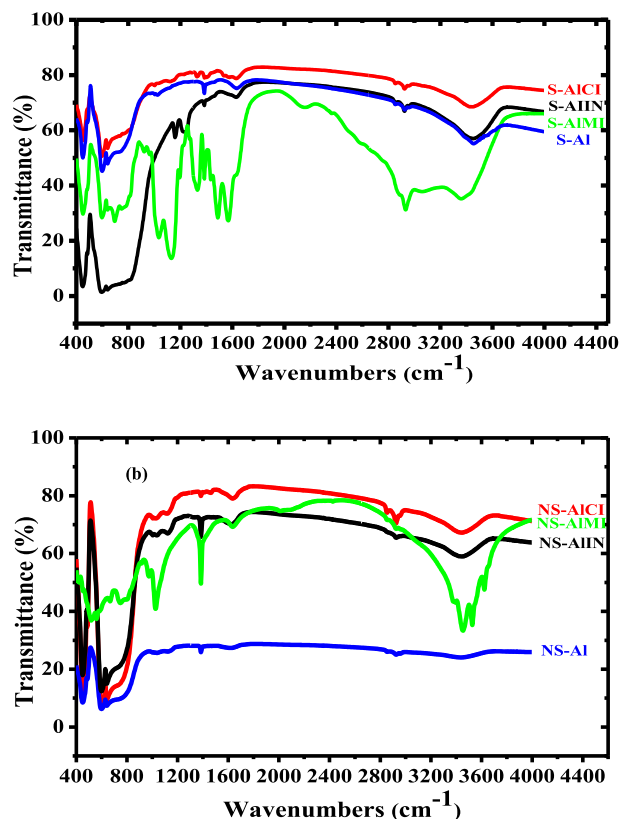$$q_e = (C_i - C_e)/w*v \quad (1)$$

$$\% A = (C_i - C_f)/C_i * 100 \quad (2)$$

where C_i, Ce and C_f are the initial, equilibrium and final concentrations of the adsorbate, respectively; w is the weight of the adsorbent (mg) and v is the volume (ml) of the adsorbate.

2.2.5. Adsorption kinetics and isotherms

Linear equations (see table 2) of adsorption kinetics such as pseudo-first-order, pseudo-second-order and intra-particle diffusion were applied to the adsorption data to determine the adsorption rate involved in the removal of lead (Pb) and mercury (Hg). Further, the adsorption isotherm of Langmuir and Freundlich was also applied to understand the adsorption mechanism [28]. The fitness of experimental data is
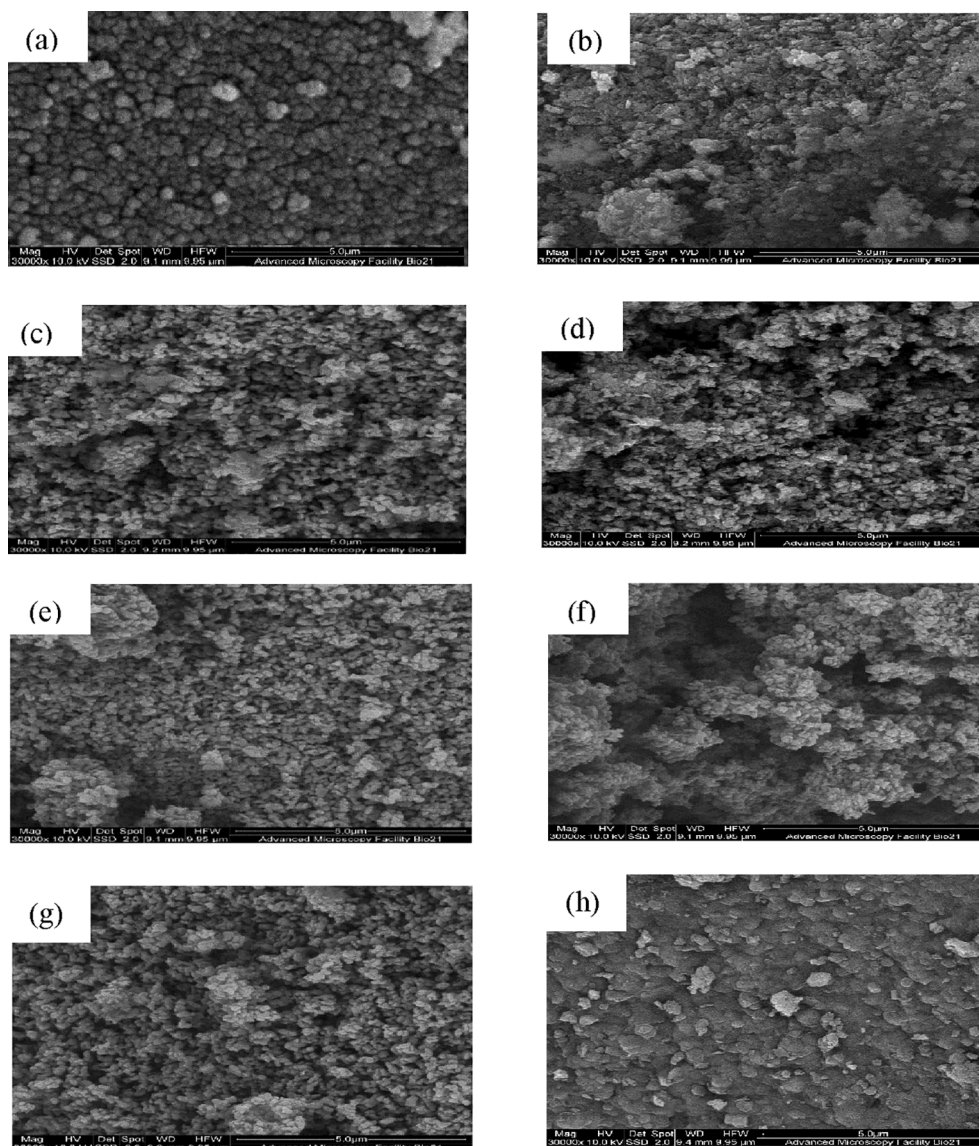

Fig. 1. FTIR spectra of aluminium oxide and aluminium hybrids synthesized from sonicated (a) and non-sonicated (b) sol gel and post grafting method.

estimated based on adsorption capacity (q_e) and regression coefficient (R^2) values.

3. Results and Discussion

The present study is an endeavor towards the synthesis of

Table 3
Percent yield and reaction time of sonicated and non-sonicated aluminium oxide and aluminium hybrids.

		Non-sonicated Aluminium Hybrids				Sonicated Aluminium Hybrids			
		NS-Al	NS-AlIN	NS-AlCl	NS-AlMI	S-Al	S-AlIN	S-AlCl	S-AlMI
Yield	Actual yield (g)	1.03	0.08	0.19	0.09	1.21	0.17	0.29	0.18
	Theoretical yield (g)	1.79	0.22	0.484	0.23	1.79	0.22	0.48	0.23
	Percent Yield (%)	57	36	39	39	68	77	60	78
Reaction time(hours)	Aluminium Oxide	24				1			
	Aluminium Hybrids	18				1			

Fig. 2. SEM of aluminium oxide and aluminium hybrids synthesized from sonicated (a = S-Al, e = S-AlIN, c = S-AlCl, g = S-Al-MI) and non-sonicated method (b = NS-Al, d = NS-AlIN, f = NS-AlCl, h = NS-Al-MI).

Table 4
BET Surface area of aluminium oxide and its hybrids from the non-sonicated and sonicated method.

Sample Code	Specific surface area (m^2/g)	Pore volume (cm^3/g)	Pore diameter (nm)
S-Al	82	0.1	8
S-AlIN	115	0.1	5
S-AlCl	167	0.1	3
S-AlMI	142	0.1	4
NS-Al	18	0.07	26
NS-AlIN	25	0.15	23
NS-AlCl	32	0.1	17
NS-AlMI	21	0.06	14

aluminium oxide and aluminium hybrids using sol–gel and post grafting assisted with sonochemical (20 kHz at 40 W) method. Sonication power is utilized for the sonolysis of the aqueous and non-aqueous solvents that resulted in radical formation. Sonication of an aqueous solution causes the growth of existing bubbles towards a resonance size range. When these cavitation bubbles implode, they generate extremely high temperatures and pressures in microscopic regions (hot spots)

accompanied by the production of primary and secondary radicals (hydrogen atoms and hydroxyl radicals). These radicals can be used to initiate the chemical reaction. In the present study, hydrogen peroxide (formed by the reaction between OH radicals) and hydroxyl radicals generated due to the sonolysis of water aid in the formation of aluminium oxyhydroxide (see Reactions 1 and 2). On the other hand, the sonolysis of non-aqueous solvents (dichloromethane) generates radicals such as methyl, methylene chloride which help in the abstraction of hydrogen from the amine-functionalized aluminium oxide. The abstraction of hydrogen creates binding sites for incoming heterocyclic compounds (indole and its derivatives). Thus, the aluminium hybrids are synthesized (see Reaction 4). For comparison, the aluminium oxide and aluminium hybrids are also synthesized using the sol–gel method without sonication. When we compared the product yield and reaction time of both sonicated and non-sonicated reactions; the sonicated reaction showed better yield in less reaction time (see table 3). The sonication energy has high power which mediates the chemical reaction faster (due to the consumption of available radicles) and produces a good yield. Thus it reduces the reaction time from days to the hours. The non-sonicated method is a slow process and took a day for Ostwald ripening. Hence, the sonochemical assisted sol–gel is proved as an
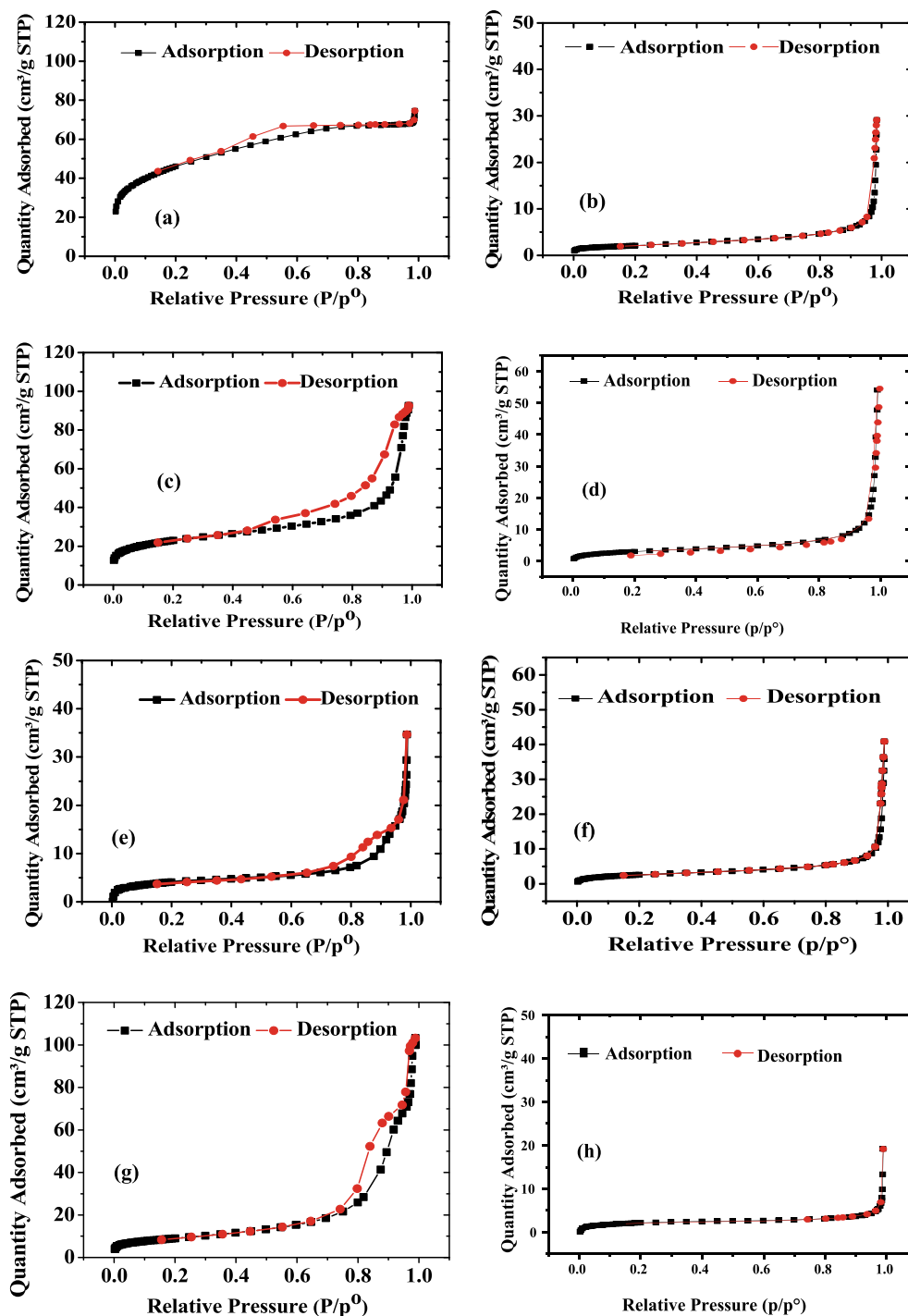
Fig. 3. BET curve of aluminium-indole hybrids synthesized from non-sonicated (a = S-Al, e = S-AlIN, c = S-AlCI, g = S-Al-MI) and sonicated method (b = NS-Al, d = NS-AlIN, f = NS-AlCI, h = NS-Al-MI).

efficient and environmentally benign method in comparison to the conventional sol–gel method without sonication.

The product yield was calculated using Eq. (3).

$$Percent\ Yield(\%) = actual\ yield/theoretical\ yield * 100 \quad (3)$$

3.1. FTIR

FTIR Spectra of sonicated aluminium oxide and aluminium hybrids showed distinctive absorption bands from 4000 to 400 cm^{-1} (see Fig. 1). The broad absorption bands at 3460 cm^{-1} is assigned to stretching vibration of the hydroxyl group attached with aluminium (Al-OH) [29].

While multiple absorption bands between 1000 and 400 cm^{-1} are assigned to aluminium oxide (Al-O, Al-O-Al). When aluminium oxide is hybridized with indole and its derivatives, new absorption bands emerged in a different region. The absorption bands of -C = C at 1485 cm^{-1}, –CN at 1340–1122 cm^{-1}, C-O(COOH) at 1325–1224 cm^{-1} and –NH at 1625–1562 cm^{-1} confirmed the attachment of indole and its derivatives with repeating units of aluminium matrix (Al-O-Al). The coordination of different metals with indole groups have been reported by Liu et al. [30] and Gomez et al., [31]. It is noticed that the benzene ring (C–C, C = C) of indole has not been affected by hybrid synthesis [32,33] and the synthesis of hybrids occurred via C$_2$ and C$_3$ of pyrrole ring of indole due to high electron density. Furthermore, methyl and
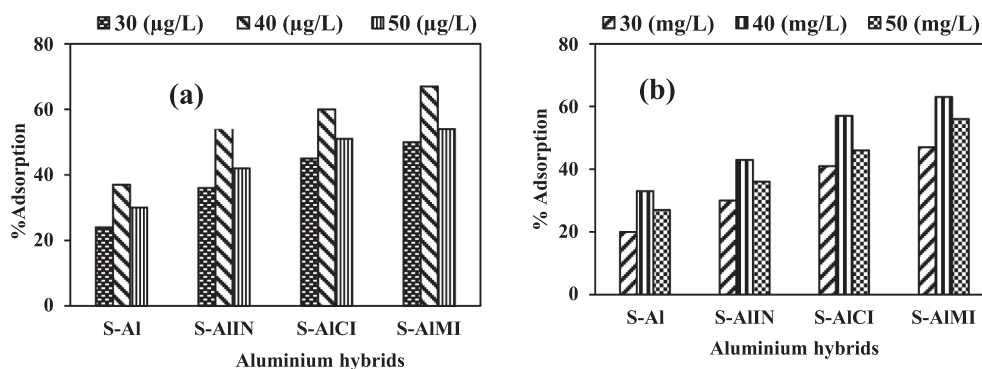
Fig. 4. Adsorption of (a) mercury and (b) lead as a function of concentration using sonicated aluminium oxide and aluminium hybrids.
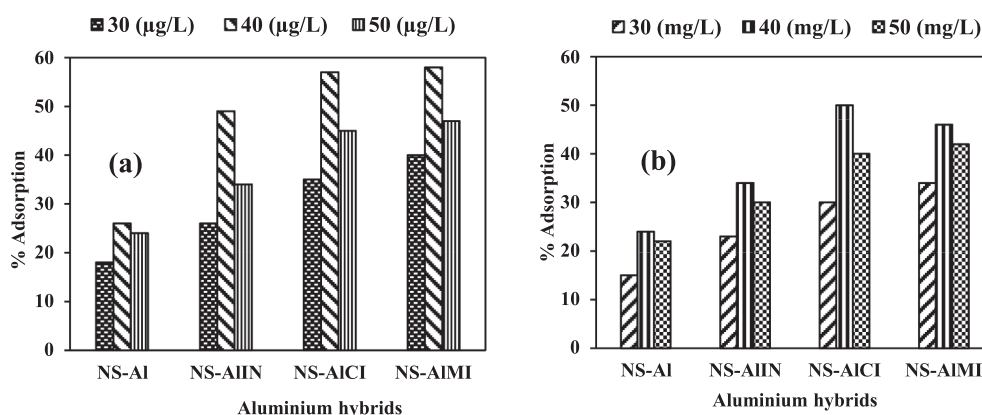

Fig. 5. Adsorption of (a) mercury and (b) lead as a function of concentration using non-sonicated aluminium oxide and aluminium hybrids.
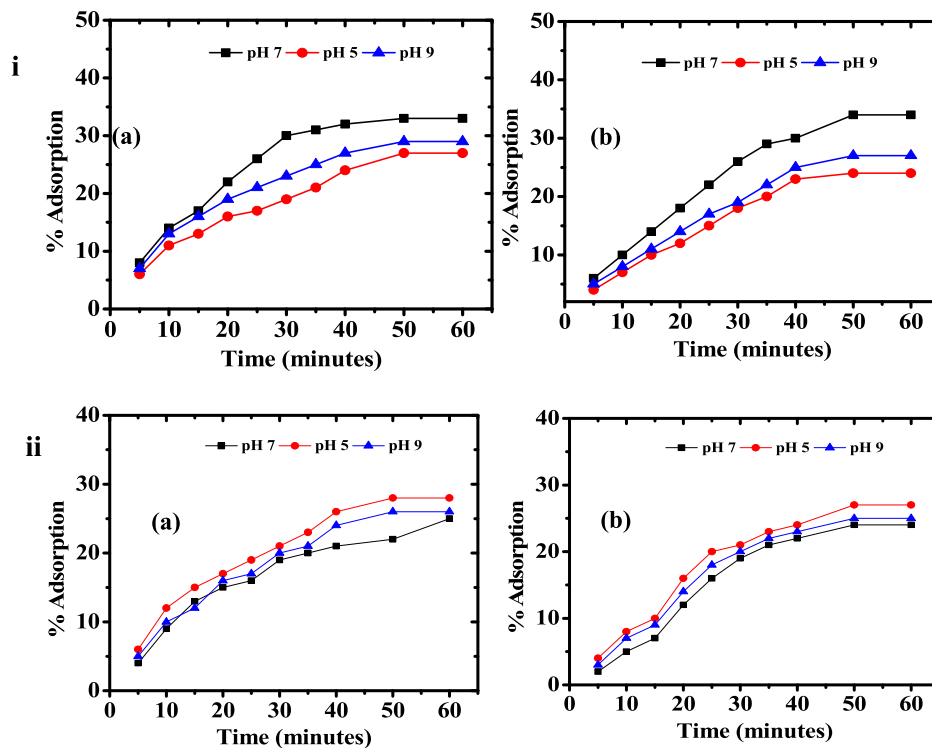
Fig. 6. Sonicated aluminium (i) and Non-sonicated (ii) aluminium oxide as an adsorbent for (a) Mercury and (b) Lead.

carboxylic substituted indole at C$_2$ position provide an additional site for attachment. Similarly, in the case of non-sonicated synthesized aluminium and aluminium hybrids, all respective absorption bands are observed with less intensity. Less intense absorption bands infer the less participation of indole groups in hybrid synthesis. Hence, it is observed that the absorption band of sonicated treated aluminium oxide and aluminium hybrids are well defined and sharp, indicating the good integration of indole and its derivatives.
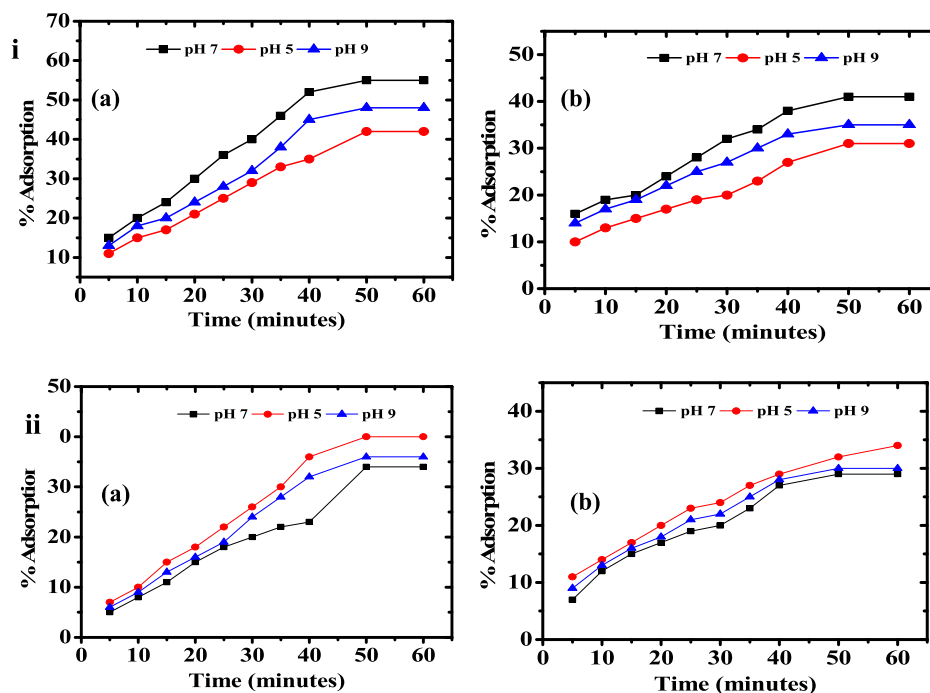
Fig. 7. Sonicated (i) and Non-sonicated (ii) aluminium-indole as an adsorbent for (a) Mercury and (b) Lead.
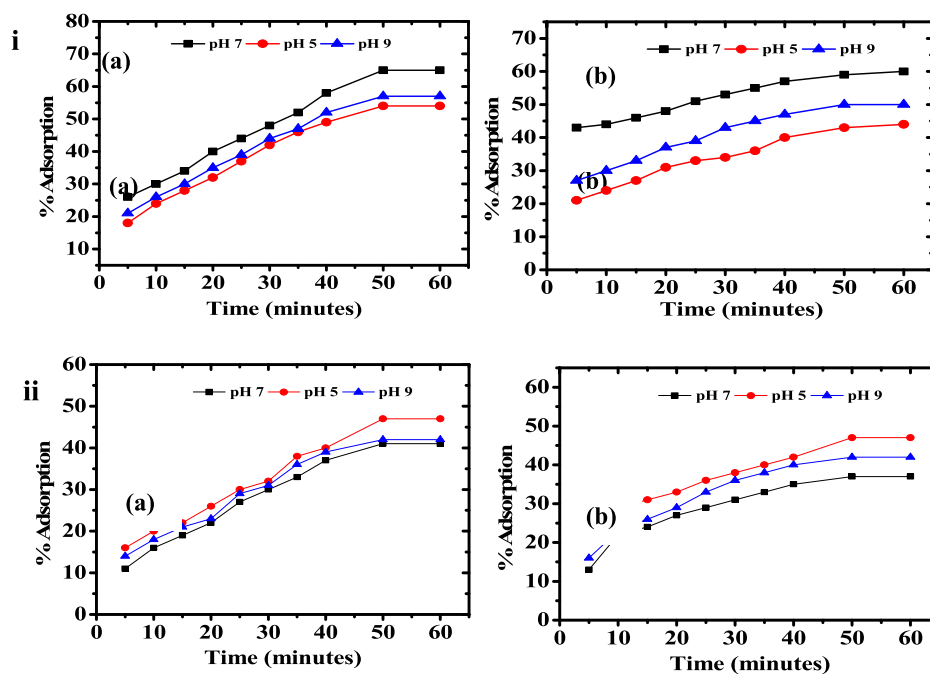

Fig. 8. Sonicated (i) and Non-sonicated (ii) aluminium-carboxylic indole hybrid as an adsorbent for (a) Mercury and (b) Lead.

3.2. SEM

SEM images of sonicated aluminium oxide showed spherical shaped clusters (see Fig. 2 (a)) in comparison to non-sonicated aluminium oxide. It is assumed that the spherical shape of particles is developed by impinging the intense physical stress as a result of the implosion of acoustic cavitation. These clusters get interconnected with each other after hybrid synthesis and form a porous structure with different particle sizes (see Fig. 2 (c, e and g)). This kind of interconnection is also observed by Krishnan et al., [34]. Furthermore, the indole derivatives provide an additional reactive point for aluminium oxide, resulting in the reorientation of particles and forms the clumps [35]. The reorientation of particles creates voids that facilitate the adsorption process. While non-sonicated aluminium hybrids showed fused and aggregated particles (see Fig. 2 (b, d, f and h)). The fusion of particles covered the interstitial spaces and block the passages, that's why only surface attachment is possible. The less incorporation of indole groups into aluminium oxide is duly supported by FTIR results.

3.3. BET:

The BET data elucidate the specific surface area while the physical adsorption–desorption of nitrogen demonstrates the pore size distribution of particles. From table 4, it is observed that sonicated aluminium oxide and aluminium hybrids show a high surface area to volume ratio in comparison
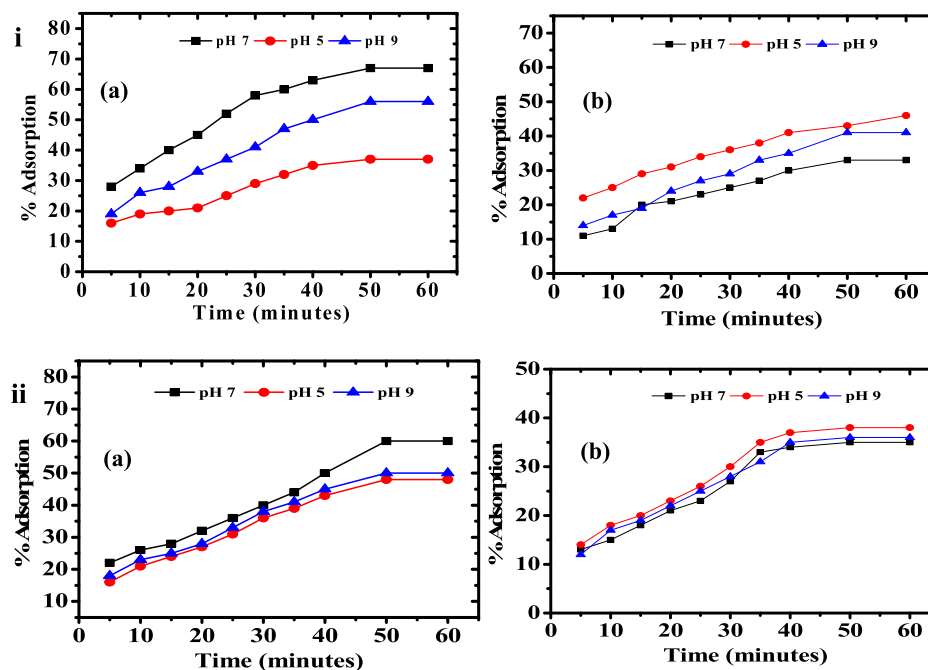
Fig. 9. Sonicated (i) and Non-sonicated (ii) and Non-sonicated aluminium-methyl indole as an adsorbent for (a) Mercury and (b) Lead.

Table 5
Kinetic Parameters on the adsorption data of mercury and lead at 40 mg/L and pH 7.

		Sonicated Aluminium oxide		Non-sonicated Aluminium oxide	
		Hg	Pb	Hg	Pb
	qe exp.(µg/g and mg/g)	6	5.6	4.2	3.4
Pseudo-first order	$K_1(min^{-1})$	1.6×10^{-2}	2×10^{-2}	1.4×10^{-2}	1.7×10^{-2}
	qe cal. (µg/g and mg/g)	4.7	7.2	4.12	2.38
	R^2	0.89	0.70	0.93	0.52
Pseudo-second order	K_2	1.7×10^{-3}	1×10^{-2}	2×10^{-1}	5.74×10^{-2}
	qe cal. (µg/g and mg/g)	13	14	2	5.3
	R^2	0.89	0.77	0.56	0.99
		Sonicated Aluminium-indole		Non-sonicated Aluminium indole	
	qe exp.(µg/g and mg/g)	7	6	5.3	4.3
Pseudo-first order	$K_1(min^{-1})$	2.1×10^{-2}	4×10^{-2}	1.7×10^{-2}	2×10^{-2}
	qe cal. (mg/g)	10	5.9	6	4.2
	R^2	0.96	0.94	0.96	0.95
Pseudo-second order	K_2	1×10^{-3}	1.2×10^{-2}	4×10^{-1}	9.2×10^{-2}
	qe cal. (mg/g)	11	10	4	6
	R^2	0.91	0.84	0.69	0.95
		Sonicated Aluminium-carboxylic indole		Non-sonicated Aluminium-carboxylic indole	
	qe exp.(µg/g and mg/g)	9	7.3	6	6.6
Pseudo-first order	$K_1(min^{-1})$	1×10^{-2}	1×10^{-2}	1.3×10^{-2}	1.5×10^{-2}
	qe cal. (mg/g)	9.7	7.7	5	4.07
	R^2	0.97	0.98	0.98	0.97
Pseudo-second order	K_2	1.3×10^{-4}	1×10^{-2}	1.1×10^{-2}	1.8×10^{-2}
	qe cal. (mg/g)	12	13	5	7
	R^2	0.96	0.89	0.88	0.98
		Sonicated Aluminium-methyl indole		Non-sonicated Aluminium-methyl indole	
	qe exp.(µg/g and mg/g)	7	6.6	5	6
Pseudo-first order	$K_1(min^{-1})$	2.2×10^{-2}	1×10^{-2}	1.8×10^{-2}	1.8×10^{-1}
	qe cal. (mg/g)	10	6	4.2	4.3
	R^2	0.96	0.89	0.95	0.96
Pseudo-second order	K_2	7×10^{-4}	2×10^{-2}	8×10^{-2}	9×10^{-2}
	qe cal. (mg/g)	13	12	7	6.6
	R^2	0.91	0.88	0.92	0.98

to non-sonicated aluminium oxide. The high surface area depicted the presence of interstitial spaces between the particles. The interstitial spaces were created by the implosion of acoustic cavitation [36,37]. The increase in the surface area confirmed the attachment of 2-methylindole (142 m²/g), indole (115 m²/g) and carboxylic acid 2-indole (167 m²/g) groups. It is assumed that attachment of indole group provides the additional surface area which facilitates the adsorption process. A similar trend was also

observed by other researchers [38,39]. The nitrogen adsorption–desorption isotherm showed adsorption type-III and IV by non-sonicated and sonicated aluminium hybrids. The BJH hysteresis loop indexed H3 which is the signature of mesoporous particles (IUPAC classification, 1985). The type-III adsorption isotherm indicates the multilayered and mesoporous structure which facilitates the only physisorption of lead and mercury. While the type-IV adsorption isotherm defined the multilayered structure likely to

Table 6

Parameters of intra-particle diffusion model on the adsorption data of mercury and lead at 40 mg/L and pH 7.

	Mercury Sonicated Aluminium oxide			Lead			Mercury Non-sonicated Aluminium oxide			Lead		
	S_1	S_2	S_E	S_1	S_2	S_E	S_1	S_2	S_E	S_1	S_2	S_E
Kid (mg/g min)	0.40	1.12	1.44	0.39	0.73	1.81	0.66	0.53	1.24	0.58	0.63	1.35
R^2	0.99	0.93	1	0.98	0.95	0.99	0.93	0.97	1	0.99	0.97	1
Sonicated Aluminium-indole							**Non-sonicated Aluminium-indole**					
C cal. (mg/g)	1.75	3.01	2.80	0.30	3.16	3.90	0.20	0.65	2.20	0.23	0.85	4.33
Kid (mg/g min)	0.86	1.45	1.49	0.76	1.27	1.29	0.40	0.67	1.40	0.53	0.63	1.19
R^2	0.98	0.99	1	0.99	0.96	1	0.97	0.98	1	0.99	0.96	1
Sonicated Aluminium-carboxylic indole							**Non-sonicated Aluminium-carboxylic indole**					
C cal. (mg/g)	0.99	1.30	1.52	1.06	1.32	1.6	0.84	1.05	1.83	0.77	1.81	1.88
Kid (mg/g min)	1.10	1.45	1.74	1.10	2.34	2.74	0.57	1.08	5.25	0.35	0.58	2.74
R^2	0.97	0.99	1	0.97	0.95	1	0.97	0.95	1	0.99	0.99	0.97
Sonicated Aluminium-methyl indole							**Non-sonicated Aluminium-methyl indole**					
C cal. (mg/g)	0.83	1.14	4.30	0.48	1.72	4.5	0.59	1.2	1.7	1.03	1.6	2.34
Kid (mg/g min)	1.06	1.45	1.6	0.08	0.88	0.85	0.56	1.10	1.33	0.63	1.09	1.53
R^2	0.98	0.99	1	0.95	0.99	0.99	0.98	0.95	1	0.97	0.99	1

Table 7

Parameters of adsorption isotherm fitted on the adsorption data of mercury and lead at 40 mg/L and pH 7.

Sonicated Aluminium oxide				Non-sonicated Aluminium oxide	
		Hg	Pb	Hg	Pb
Langmuir	qm (mg/g)	17	8	13	11
	K_L (min^{-1})	2×10^{-2}	1.5×10^{-2}	5.3×10^{-2}	1.9×10^{-2}
	R^2	0.96	0.67	0.99	0.95
Freundlich	K_F (min^{-1})	20	14	50	48
	n	1.5×10^{-1}	6×10^{-2}	4.5×10^{-1}	4.6×10^{-2}
	R^2	0.95	0.69	0.99	0.97
Sonicated Aluminium-indole				**Non-sonicated Aluminium-indole**	
Langmuir	qm (mg/g)	17	9	2	1.7
	K_L (min^{-1})	2×10^{-2}	1.6×10^{-2}	6.4×10^{-2}	5.7×10^{-2}
	R^2	0.95	0.62	0.99	0.98
Freundlich	K_F (min^{-1})	15	12	18	14
	n	1.5×10^{-1}	7×10^{-2}	5.7×10^{-1}	3.8×10^{-1}
	R^2	0.95	0.64	0.99	0.98
Sonicated Aluminium-carboxylic indole				**Non-sonicated Aluminium-carboxylic indole**	
Langmuir	qm (mg/g)	47	38	26	25
	K_L (min^{-1})	1.5×10^{-2}	8×10^{-3}	7.9×10^{-2}	7.8×10^{-2}
	R^2	0.99	0.89	0.99	0.97
Freundlich	K_F	36	16	30	32
	n	1.2×10^{-1}	9×10^{-2}	7.8×10^{-1}	7.4×10^{-1}
	R^2	0.99	0.89	0.99	0.98
Sonicated Aluminium-methyl indole				**Non-sonicated Aluminium-methyl indole**	
Langmuir	qm (mg/g)	31	26	14	25
	K_L (min^{-1})	1.6×10^{-2}	3.4×10^{-3}	1.5×10^{-2}	1.2×10^{-2}
	R^2	0.95	0.92	0.93	0.94
Freundlich	K_F	15	13	26	25
	n	8×10^{-1}	7×10^{-2}	2.4×10^{-1}	1.5×10^{-1}
	R^2	0.89	0.89	0.92	0.98

facilitate physisorption and chemisorption via capillary condensation within and outside the pores (see Fig. 3). From the above mentioned FTIR, SEM and BET results, it is confirmed that the aluminium oxide and aluminium hybrids synthesized from the sol–gel assisted sonochemical method showed better properties. Therefore, XRD and XPS of sonicated aluminium oxide and aluminium hybrids are only performed (see supplementary file).

3.4. Application of sonicated and non-sonicated aluminium oxide and aluminium hybrids:

The potential applications of sonicated and non-sonicated aluminium oxide and aluminium hybrids were investigated as an adsorbent for the removal of toxic metals (lead and mercury). Time-depended adsorption batch experiments were conducted using a known amount of adsorbent (30 mg) as a function of pH (5 as acidic, 7 as neutral, and 9 as basic), and concentrations (30 mg/L, 40 mg/L and 50 mg/L for Pb while 30 µg/L, 40 µg/L, and 50 µg/L for mercury) till equilibrium is attained.

3.4.1. Influence of initial concentration:

The influence of initial concentration on the adsorption of lead (Pb) and mercury (Hg) are studied and presented in Figs. 4 and 5. It is found that adsorption of lead (Pb) and mercury (Hg) increase with an increase in time because initially adsorbent sites are vacant and the concentration gradient is high [40]. As the adsorbent sites are filled the adsorption process leveled off and stopped. It is also noted that the increase in

Table 8
RL values calculated for the adsorption of mercury and lead.

Sonicated aluminium oxide and aluminium hybrids				
Mercury				
Initial concentration (μg/L)	**A**	**AI**	**ACI**	**AMI**
30	0.62	0.55	0.68	0.67
40	0.55	0.48	0.62	0.60
50	0.50	0.42	0.56	0.55
Initial concentration (mg/L)	**Lead**			
30	0.68	0.68	0.80	0.49
40	0.62	0.61	0.75	0.42
50	0.56	0.55	0.71	0.37
Non-sonicated aluminium oxide and aluminium hybrids				
Initial concentration (μg/L)	**Mercury**			
30	0.40	0.36	0.29	0.38
40	0.32	0.30	0.24	0.31
50	0.27	0.25	0.20	0.26
Initial concentration (mg/L)	**Lead**			
30	0.14	0.34	0.29	0.28
40	0.11	0.28	0.24	0.23
50	0.09	0.23	0.20	0.19

the induced concentration from 30 mg/L to 40 mg/L for Lead or 30 μg/L to 40 μg/L for mercury, increases the metal ion adsorption because of space available on the adsorbent surface. It is observed that a further increase in induced concentration (50 mg/L for Lead and 50 μg/L for mercury) decrease the adsorption. It is due to a fixed number of sufficient adsorbent sites which is already saturated (see Fig. 4). Thus, the maximum adsorption is found at 40 mg/L for lead and 40 μg/L for mercury that were selected for further investigation on varying pH. The equilibrium attainment is noted within 60 min. A similar adsorption trend is observed in the adsorption of lead and mercury using non-sonicated aluminium oxide and aluminium hybrids (see Fig. 5).

3.4.2. Influence of pH:

The influence of pH on the adsorption of lead (Pb) and mercury (Hg) is studied and presented in Figs. 6-13. It is noted that adsorption of lead and mercury is generally higher at pH 7 in comparison to pH 5 (acidic) and pH 9 (alkaline). Low adsorption of Pb and Hg at pH 5 is due to the presence of hydronium ion (H_3O^+) in competition with lead or mercury ion to cover the adsorbent site. On the other hand, hydronium ion (H_3O^+) concentration decreases at pH 7 offering more adsorbent sites to lead and mercury for adsorption. The decline in adsorption at pH 9 is associated with precipitation of metal ion with anion (hydroxide) into solution. Thus the pH variation followed the general trend (pH7 > pH5 > pH9). Similar results have been reported previously [41]. Different types of adsorbents showed different behavior toward different metals, based on surface chemistry. The sonicated aluminium oxide showed 37% and 33% adsorption of mercury and lead, while non-sonicated aluminium oxide showed 26% and 24% adsorption of mercury and lead (see Fig. 6). It can be seen that the sonicated treated aluminium oxide showed relatively better adsorption of metals due to its high surface area to volume ratio in comparison to non-sonicated aluminium oxide.

Fig. 7. show sonicated aluminium-indole hybrid adsorbed 55% mercury and 43% lead at pH 7 in comparison to non-sonicated aluminium-indole 49% and 34% of mercury and lead, respectively. A similar trend is observed for other derived hybrid i.e., aluminium-carboxylic indole and aluminum-methyl indole, as shown in figure (see Figs. 8 and 9). The sonicated aluminium-carboxylic indole showed 60% and 57% removal of mercury and lead while sonicated aluminum-methyl indole showed 67% and 63% removal of mercury and lead. The non-sonicated aluminium-carboxylic indole showed 57% and 50% removal of mercury and lead while sonicated aluminum-methyl indole showed 58% and 46% removal of mercury and lead. It is also likely to mention that

aluminium hybrid showed better adsorption potential towards mercury and lead than aluminium oxide due to the synergetic effect of organic–inorganic moieties [42]. It is very interesting to note that the adsorption of mercury is relatively higher than lead due to its smaller ionic radii (102 pm) and lower hydration enthalpy (-1829kj/mol) than lead (119 pm, −1485kj/mol) which help to diffuse in and on the particles.

3.5. Adsorption kinetics and Isotherms:

Linear equations of adsorption kinetics (pseudo-first-order, pseudo-second-order, and intra-particle diffusion) and adsorption isotherms (Freundlich and Langmuir) have been applied to experimental data. The applied kinetics and isotherms helped in the determination of the adsorption rate and adsorption mechanism involved in the removal of Pb and Hg using sonicated and non–sonicated synthesized aluminium oxide and aluminium hybrids [28]. The fitness of experimental data is estimated based on adsorption capacity (q_e) and regression coefficient (R^2) values.

Table 2 shows the kinetic parameters of pseudo-first and pseudo-second-order on the adsorption of experimental data. Both kinetics (pseudo-first-order and pseudo-second-order models) are fitted well on the experimental data with the value of R^2 close to 1 for Hg and Pb. The sonicated and non-sonicated synthesized aluminium oxide and aluminium hybrids showed more coherence towards mercury with potential adsorption capacity in comparison to the lead metal ion. Due to the small size of mercury, initially, it started the physio-sorption followed by chemisorption. While lead showed more inclination toward physisorption. It can be witnessed by comparing the value of regression as presented in table 5 that less deviation and more closeness between the experimental and calculated adsorption capacity (q_e) present a good correlation. The findings of the present research are further strengthened by other studies [42]. Application of the intra-particle diffusion [42] shows that the adsorption occurs through diffusion in two steps followed by equilibrium or saturation of adsorbent surface (see table 6). The rapid diffusion of adsorbate in the first step is evident that it is governed by physicochemical forces. Whereas, adsorption is mostly controlled in a second step defining it as a rate-limiting step. The calculated diffusion coefficient (K_{id}) values indicate the deviation from the linear relationship between qt versus time. A higher K_{id} suggested more than one rate-controlling step.

Minimum and maximum values of intercepts (C) calculated for Hg and Pb suggest that the boundary layer thickness is higher for lead adsorption that restricted its movement in comparison to the mercury.

Elucidation of Langmuir and Freundlich models [43] fitted on adsorption data are summarized in Table 7. The result of Langmuir parameters (qm, K_L) refers to the distribution of adsorbed molecules between the liquid and solid phases under equilibrium. On the other hand, Freundlich parameters (n and K_F) refers to adsorption intensity and capacity which can easily be calculated from intercept and slope.

Further probing revealed that the qm of mercury (17–47 mg/g) is higher than lead (8–38 mg/g) which represented the monolayer coverage. The uptake rate K_L $(1.5 \times 10^{-2} - 2 \times 10^{-2})$ of mercury per minute was also higher than lead as shown in table 7. Regarding the Freundlich model, a higher value of n $(1.2 \times 10^{-1} - 8 \times 10^{-2})$ is found for Hg, indicating that Hg uptake on hybrids is more than Pb (n = $6 \times 10^{-2} - 9 \times 10^{-2}$). Similarly, K_F (min^{-1}) for mercury is higher than lead. The value of correlation coefficient (R^2 is close to 1) shows that both adsorption isotherms (Langmuir and Freundlich) are fitted well on the adsorption data. The same trend is observed for non-sonicated synthesized aluminium oxide and aluminium hybrids. Therefore, it can be concluded that the adsorption of lead and mercury on the sonicated and non-sonicated synthesized aluminium hybrids is a good combination of mono sublayer leading to multilayer adsorption.

The separation factor "R_L" (values ranging from 0 to 1) also signifies whether the adsorption process is favorable or unfavorable and

reversible or irreversible. It is calculated using equation 4.

$$R_L = 1/(1 + K_L C_i) \tag{4}$$

Upon considering the R_L values (table 8), it can be assessed that adsorption is a favorable process under optimum conditions because all the values are between 0 and 1. The R_L value equal to 1 is assigned to the linear and reversible process [44]. If R_L value is equal to 0 or more than 1, then the adsorption process become irreversible and unfavorable.

4. Conclusions

Aluminium oxide and aluminium hybrids have been successfully synthesized using the sol–gel assisted sonochemical method and are used as adsorbents for the adsorption of lead and mercury. The optimum adsorption of lead and mercury is attained at 40 mg/L and pH 7 within an equilibrium contact time of 1 h. The sonicated treated aluminium hybrids showed better adsorption potential of mercury and lead up to 67% and 63%, respectively, in comparison to non-sonicated treated aluminium hybrids (58% for mercury and 50% for lead). Thus the adsorption process is governed by pseudo-first-order, pseudo-second-order, Langmuir and Freundlich isotherm with the regression coefficient (R^2) greater than 0.99.

CRediT authorship contribution statement

Kousar Parveen: Investigation, Writing - original draft. **Uzaira Rafique:** Supervision, Conceptualization, Visualization. **Muhammad Javed Akhtar:** Formal analysis, Validation. **Muthupandian Ashokkumar:** Supervision, Resources, Writing - review & editing.

Declaration of Competing Interest

The authors declare that they have no known competing financial interests or personal relationships that could have appeared to influence the work reported in this paper.

Acknowledgement

Appendix A. Supplementary data

Supplementary data to this article can be found online at https://doi.org/10.1016/j.ultsonch.2020.105299.

References:

[1] A. Waseem, J. Arshad, F. Iqbal, A. Sajjad, Z. Mehmood, G. Murtaza, Pollution status of Pakistan: a retrospective review on heavy metal contamination of water, soil, and vegetables, Biomed. Res. Int. 1–29 (2014) 813206, , https://doi.org/10.1155/2014/813206.

[2] M.A. Khwaja, A. Aslam, Comparative assessment of pakistan national drinking water quality standards with selected asian countries and world health organization, first, Sustainable Development Policy Institute, Pakistan, 2018 https://think-asia.org/handle/11540/8388.

[3] F. Fu, Q. Wang, Removal of heavy metal ions from wastewaters: a review, J. Environ. Manage. 92 (2011) 407–418, https://doi.org/10.1016/j.jenvman.2010.11.011.

[4] M.S.M. Yusoff, M. Muslimin, Synthesis of alumina using the solvothermal method, Malaysian, J. Anal. Sci. 11 (2007) 262–268.

[5] A. Mekki-Berrada, D. Grondin, S. Bennici, A. Auroux, Design of amphoteric mixed oxides of zinc and Group 3 elements (Al, Ga, In): migration effects on basic features, Phys. Chem. Chem. Phys. 14 (2012) 4155–4161 http://doi=10.1039/C2CP23613C.

[6] A. Rajaeiyan, M.M. Bagheri-Mohagheghi, Comparison of sol-gel and co-precipitation methods on the structural properties and phase transformation of γ and α-Al2O3 nanoparticles, Adv. Manuf. 1 (2013) 176–182 http://doi=10.1007/s40436-013-0018-1.

[7] M. Farahmandjou, N. Golabiyan, Synthesis, and characterization of Alumina (Al, Int. J. Bio-Inorg. Hybr. Nanomater, 5 (2016) 73-77. http://doi=_44e2c1f3afc8a-d56378a4c07ee84e255.

[8] L. Yang, S. Yin, T. Sato, Synthesis of morphology controlled aluminium oxide by the hydrothermal reaction, in, IOP Conference Series: Mater. Sci. Eng., IOP Publishing (2011) 032015.

[9] B. Ebin, S. Gurmen, Nanotechnology: Synthesis of alumina nanoparticles by heat treatment of thermal decomposed aluminium sulfate aerosol droplets, in: european congress and exhibition on powder metallurgy, The European Powder Metallurgy Association, 2010, pp.1.

[10] A. Tavakoli, M. Sohrabi, A. Kargari, A review of methods for synthesis of nanostructured metals with emphasis on iron compounds, Chem. Pap. 61 (2007) 151–170, https://doi.org/10.2478/s11696-007-0014-7.

[11] H. Xu, B.W. Zeiger, K.S. Suslick, Sonochemical synthesis of nanomaterials, Chem. Soc. Rev. 42 (2013) 2555–2567, https://doi.org/10.1039/c2cs35282f.

[12] K.S. Suslick, Kirk-Othmer encyclopedia of chemical technology, John Wiley & Sons, New York, 1998.

[13] E. Luévano-Hipólito, L. Torres-Martínez, Sonochemical synthesis of ZnO nanoparticles and its use as photocatalyst in H₂ generation, Mater. Sci. Eng: B 226 (2017) 223–233, https://doi.org/10.1016/j.mseb.2017.09.023.

[14] A. Hassanjani-Roshan, M.R. Vaezi, A. Shokuhfar, Z. Rajabali, Synthesis of iron oxide nanoparticles via sonochemical method and their characterization, Particuology 9 (2011) 95–99, https://doi.org/10.1016/j.partic.2010.05.013.

[15] Y. Cui, D. Zhou, Z. Sui, B. Han, Sonochemical synthesis of graphene oxide-wrapped gold nanoparticles hybrid materials: visible light photocatalytic activity, Chin. J. Chem. 33 (1) (2015) 119–124, https://doi.org/10.1002/cjoc.201400309.

[16] G.J. Lee, X.Y. Lee, C. Lyu, N. Liu, S. Andandan, J.J. Wu, Sonochemical synthesis of copper-doped BiVO₄/g-C₃N₄ nanocomposite materials for photocatalytic degradation of Bisphenol A under simulated sunlight irradiation, Nanomater. 10 (3) (2020) 498, https://doi.org/10.3390/nano10030498.

[17] A.S. Dezfuli, M.R. Ganjali, P. Norouzi, F. Faridbod, Facile sonochemical synthesis and electrochemical investigation of ceria/graphene nanocomposites, J. Mater. Chem. B 3 (11) (2015) 2362–2370, https://doi.org/10.1039/c4tb01847h.

[18] E.C. Gaudino, M. Manzoli, D. Carnaroglio, Z. Wu, G. Grillo, L. Rotolo, J. Medlock, W. Bonrath, G. Cravotto, Sonochemical preparation of alumina-spheres loaded with Pd nanoparticles for 2-butyne-1, 4-diol semi-hydrogenation in a continuous flow microwave reactor, RSC Adv. 8 (2018) 7029–7039, https://doi.org/10.1039/C8RA00331A.

[19] T. Chave, S.I. Nikitenko, D. Granier, T. Zemb, Sonochemical reactions with mesoporous alumina, Ultrason. Sonochem. 16 (4) (2009) 481–487, https://doi.org/10.1016/j.ultsonch.2008.12.015.

[20] W. Lv, B. Liu, Q. Qiu, F. Wang, Z. Luo, P. Zhang, S. Wei, Synthesis, characterization and photocatalytic properties of spinel CuAl₂O₄ nanoparticles by a sonochemical method, J. Alloys and Compd. 479 (1–2) (2009) 480–483, https://doi.org/10.1016/j.jallcom.2008.12.111.

[21] M. Nazari, R. Halladj, Adsorptive removal of fluoride ions from aqueous solution by using sonochemically synthesized nanomagnesia/alumina adsorbents: an experimental and modeling study, J. Taiwan Inst. Chem. Eng. 45 (5) (2014) 2518–2525, https://doi.org/10.1016/j.jtice.2014.05.020.

[22] F.M. Segal, M.F. Correa, R. Bacani, B. Castanheira, M.J. Politi, S. Brochsztain, E.R. Triboni, A novel synthesis route of mesoporous γ-alumina from polyoxohydroxide aluminum, Mater. Res. 21 (2018) 1, https://doi.org/10.1590/1980-5373-mr-2017-0674.

[23] M.A. Philip, U. Natarajan, R. Nagarajan, Acoustically-enhanced particle dispersion in polystyrene/alumina nanocomposites, Adv. Nano Res 2 (2) (2014) 121 https://doi.org/10.12989/anr.2014.2.2.121.

[24] Q. Wang, P. Chen, X. Zeng, H. Jiang, F. Meng, X. Li, X. Luo, Synthesis of (ZrO₂-Al₂O₃)/GO nanocomposite by sonochemical method and the mechanism analysis of its high defluoridation, J. Hazard. Mater. 381 (2020) 120954 https://doi.org/10.1016/j.jhazmat.2019.120954.

[25] M. Ameen, M.T. Azizan, A. Ramli, S. Yusup, M. Yasir, Physicochemical properties of Ni-Mo/γ-Al₂O₃ catalysts synthesized via sonochemical method, Pro Eng. 148 (2016) 64–71, https://doi.org/10.1016/j.proeng.2016.06.496.

[26] S. Kango, S. Kalia, A. Celli, J. Njuguna, Y. Habibi, R. Kumar, Surface modification of inorganic nanoparticles for development of organic–inorganic nanocomposites-A review, Prog. Polym. Sci. 38 (2013) 1232–1261, https://doi.org/10.1016/j.progpolymsci.2013.02.003.

[27] A.F. de Melo Pinheiro, A. Nijmeijer, V.G.P. Sripathi, L. Winnubst, Chemical modification/grafting of mesoporous alumina with polydimethylsiloxane (PDMS), Eur. J. Chem. 6 (2015) 287–295, https://doi.org/10.5155/eurjchem.6.3.287-295.1258.

[28] O. Olaofe, S. Olagboye, P. Akanji, E. Adamolugbe, O. Fowowe, A. Olaniyi, Kinetic studies of adsorption of heavy metals on clays, Int. J. Chem. 7 (2014) 48, https://doi.org/10.5539/ijc.v7n1p48.

[29] A. Rabiee, H. Baharvand, An organic-inorganic polymeric alumina hybrid nanocomposite, Polym. Sci. Ser. B. 57 (2015) 264–273, https://doi.org/10.1134/S1560090415030069.

[30] B.H. Liu, L.T. Dou, F. He, J. Yang, Z.P. Li, A cobalt coordination compound with indole acetic acid for fabrication of a high performance cathode catalyst in fuel cells, RSC Adv. 6 (2016) 19025–19033, https://doi.org/10.1039/C5RA27558J.

[31] M.B. Gómez Costa, J.M. Juárez, M.L. Martínez, J. Cussa, O.A. Anunziata, Synthesis and characterization of a novel composite: Polyindole included in nanostructured Al-MCM-41 material, Micropor. Mesopor. Mater. 153 (2012) 191–197, https://doi.org/10.1016/j.micromeso.2011.12.044.

[32] L. Joshi, R. Prakash, Polyindole-Au nanocomposite produced at the liquid/liquid interface, Mater. Lett. 66 (2012) 250–253, https://doi.org/10.1016/j.matlet.2011.08.087.

[33] L. Joshi, A.K. Singh, R. Prakash, Polyindole/ carboxylated-multiwall carbon nanotube composites produced by in-situ and interfacial polymerization, Mater. Chem. Phys. 135 (2012) 80–87, https://doi.org/10.1016/j.matchemphys.2012.04.026.

[34] S.V. Krishnan, S. Palanivelu, M.M.M. Ambalam, R. Venkatesan, M. Arivalagan,

J.M. Pearce, J. Mayandi, Chemical Synthesis and Characterization of Nano Alumina, Nano Composite of Carbon-Alumina and Their Comparative Studies, Z. Phys. Chem. 232 (12) (2018) 1827–1842, https://doi.org/10.1515/zpch-2017-1075.

[35] P. Kathirvel, J. Chandrasekaran, D. Manoharan, S. Kumar, Preparation and characterization of alpha alumina nanoparticles by in-flight oxidation of flame synthesis, J. Alloys Compd. 590 (2014) 341–345, https://doi.org/10.1016/j.jallcom.2013.12.105.

[36] C.-Y. Zuo, Q.-S. Li, G.-R. Peng, G.-Z. Xing, Manufacture of biomorphic Al2O3 ceramics using filter paper as template, Progress in Natural Science, Mater. Int. 21 (2011) 455–459, https://doi.org/10.1016/S1002-0071(12)60082-3.

[37] P.K. Kiyohara, H.S. Santos, A.C.V. Coelho, P.D.S. Santos, Structure, surface area and morphology of aluminas from thermal decomposition of Al (OH)(CH₃COO)₂ crystals, An. Acad. Bras. Ciên. 72 (2000) 471–495, https://doi.org/10.1590/S0001-37652000000400003.

[38] A. Stein, B.J. Melde, R.C. Schroden, Hybrid inorganic–organic mesoporous silicates—nanoscopic reactors coming of age, Adv. Mater. 12 (2000) 1403–1419, https://doi.org/10.1002/1521-4095(200010)12.

[39] M. Ikram, Z. Tao, J. Ye, H.A. Qayyum, X. Sun, J. Xu, Enhanced physical properties of γ-Al 2 O 3–rGO hybrids prepared by solvothermal and hot-press processing, RSC Adv. 8 (2018) 8329–8337, https://doi.org/10.1039/C8RA00095F.

[40] Q. Zhai, Nano α-Al2O3 for removal of hg (II) from water: adsorption and desorption studies, J. Chem. Pharm. Res. 6 (2014) 1310–1317 http://jocpr.com/vol6-iss5-2014/JCPR-2014-6-5-1310-1317.

[41] M.A.A. Ganzagh, M. Yousefpour, Z. Taherian, The removal of mercury (II) from water by Ag supported on nanomesoporous silica, J. Chem. Bio. 9 (2016) 127–142 https://link.springer.com/article/10.1007/s12154-016-0157-5.

[42] M. Liu, L.-A. Hou, B. Xi, Y. Zhao, X. Xia, Synthesis, characterization, and mercury adsorption properties of hybrid mesoporous aluminosilicate sieve prepared with fly ash, Appl. Surf. Sci. 273 (2013) 706–716, https://doi.org/10.1016/j.apsusc.2013.02.116.

[43] A.K. Kushwaha, N. Gupta, M. Chattopadhyaya, Adsorption behavior of lead onto a new class of functionalized silica gel, Arab. J. Chem. 10 (2017) S81–S89, https://doi.org/10.1016/j.arabjc.2012.06.010.

[44] M.L.F.A. De Castro, M.L.B. Abad, D.A.G. Sumalinog, R.R.M. Abarca, P. Paoprasert, M.D.G. de Luna, Adsorption of Methylene Blue dye and Cu (II) ions on EDTA-modified bentonite: Isotherm, kinetic and thermodynamic studies, Sustain. Environ. Res. (2018), https://doi.org/10.1016/j.serj.2018.04.001.